Nuclear Materials and Energy 36 (2023) 101491

Contents lists available at ScienceDirect

Nuclear Materials and Energy

journal homepage: www.elsevier.com/locate/nme

Experimental electronic stopping cross-section of tungsten bulk and sputter-deposited thin films for slow protons, deuterons and helium ions

Jila Shams-Latifi [a,*], Eduardo Pitthan [a], Philipp Mika Wolf [a], Daniel Primetzhofer [a,b]

[a] Department of Physics and Astronomy, Uppsala University, Box 516, SE-751 20 Uppsala, Sweden
[b] Tandem Laboratory, Uppsala University, Box 529, SE-751 21 Uppsala, Sweden

ARTICLE INFO

Keywords:
ToF-LEIS
Tungsten
Electronic stopping cross-section
In-situ
TRBS

ABSTRACT

The experimental electronic stopping cross-section of tungsten for low-energy protons, deuterons, and helium ions is deduced from backscattering experiments from thin films and bulk using time-of-flight low-energy ion scattering (ToF-LEIS). Two complementary experimental approaches showed consistent results in the energy ranges of 0.3–10 keV for protons, 0.33–10 keV for deuterons, and 0.7–10 keV for He^+ ions. In relative measurements, a Au sample was used as the reference, while in absolute energy loss measurements, sputter-deposited thin films of tungsten on carbon substrates were employed. The experimental energy-converted spectra were compared to Monte-Carlo simulations in both approaches for quantitative analysis taking the influence of plural and multiple scattering into account. The results show proportionality to the ion velocity. We discuss the present datasets in comparison to semiempirical modelling and predictions from theory.

Introduction

The interaction of energetic plasma species with materials is highly relevant for a number of research fields such as sputter deposition or materials modification expected for the plasma-facing materials in envisioned fusion devices [1]. To meet the high-heat-flux requirement of power exhaust in the divertor of the demonstration reactor (DEMO), tungsten is considered to be an armor material exposed to high fluxes of fuel species and fusion ashes [2]. A key input quantity for simulating processes such as implantation or induced collision cascades leading to sputtering is the electronic stopping power of tungsten for plasma species undergoing the aforementioned processes [3,4]. Thus, accurate knowledge of the specific energy loss of the constituents of fusion plasma in plasma-facing materials such as tungsten is essential to estimate the induced damage to the corresponding components from e.g. sputtering and other near-surface modification processes. Experimental reference data in the relevant energy range (<10 keV) is completely absent [5] and only extrapolations using semiempirical models such as SRIM [6] or predictions using different theoretical models are available. Generally applicable theoretical models around and below the stopping maximum are available, however, accurate prediction is often found difficult [7,8]. More specific, system-dependent modeling including the specific inner shell structures is possible but is found much more demanding [9–12].

To provide experimental reference data, and thus to benchmark predictions and improve the accuracy of semiempirical models, in this work, the electronic stopping cross-section (SCS, ε) of tungsten bulk and sputter-deposited thin films for slow protons, deuterons and helium ions are measured using the time-of-flight low-energy ion scattering (ToF-LEIS) setup at Tandem Laboratory, Uppsala University [13]. Two complementary approaches were taken in these experiments; relative measurements on bulk W to bulk Au as a reference sample, and absolute measurements on sputter-deposited thin films of W.

Methods

Sample preparation

We prepared two different sets of targets, depending on the experimental approach. We used bulk tungsten with a thickness of ca. 0.05 mm from Plansee in the relative measurements employing bulk gold with 0.1 mm thickness and 99.9975% purity from Alfa Aesar as the reference sample. Both W and Au samples were cut in approximately 5×10 mm^2 and mounted adjacent to each other on the sample holder of the ToF-LEIS system, forming a square array of 10×10 mm^2. The samples were mounted having both surfaces as level as possible with each other,

* Corresponding author.
E-mail address: jila.shams@physics.uu.se (J. Shams-Latifi).

https://doi.org/10.1016/j.nme.2023.101491
Received 28 June 2023; Received in revised form 16 August 2023; Accepted 21 August 2023
Available online 22 August 2023

ensuring the same solid angle for detected backscattering ions. After loading the sample into the preparation chamber of the ToF-LEIS system, Auger Electron Spectroscopy (AES) was used to assess the surface contaminants followed by sputter cleaning using 3 keV Ar^+ beam at an angle of 30° with respect to the surface normal with an average fluence of 0.43×10^{15} mm^{-2}. Before in-situ transferring the sample in UHV to the scattering chamber, additional AES was performed to qualitatively assess the amount of surface contaminants showing the removal of carbon and a significant reduction in the amount of oxygen.

In the absolute measurements, magnetron sputter-deposited thin films from a tungsten target (nominal purity of 99.999% from Testbourne) on carbon and silicon substrates at room temperature were employed using a PreVac magnetron sputtering system. The base pressure of the deposition chamber was around 8×10^{-8} mbar. Depositions were performed in the Ar atmosphere with a pressure of 5.6×10^{-3} mbar and a gas flow rate of 10 standard cubic centimeters per minute (sccm) with a DC power of 50 W. To increase the uniformity of the produced films, the substrates were rotated with an angular frequency of 10°/s during deposition. To remove contaminants from the target surface, pre-sputtering was done against a shutter for 2–3 min before each deposition. The deposition rate was estimated to be 5 nm/min by a Quartz Crystal Microbalance (QCM) in the system taking the nominal density of tungsten. The produced films from different deposition rounds featured thicknesses in the range of 1.9 – 18 nm quantified by Rutherford Backscattering Spectrometry (RBS) using 2 MeV He^+ ions at the 5 MV pelletron at the Tandem Laboratory of Uppsala University [14]. The purity of the thin films in the bulk has been measured to be around 99.7% by time-of-flight-energy elastic recoil detection analysis (ToF-E ERDA) using a 36 MeV I^{8+} beam at the same accelerator [15], while W and Au bulk used in the relative approach presented a 99.7% and 99.3% of purity, respectively. Each sample was loaded into the preparation chamber immediately after being deposited ex-situ. The preparation procedure consisted of an AES measurement, and then one round of 3 keV Ar^+ sputtering with an average fluence of 0.7×10^{14} mm^{-2}. The last AES measurement showed the removal of carbon and a significant reduction in the amount of oxygen. After transferring the sample to the scattering chamber with a base pressure of approximately 8×10^{-10} mbar, no further treatment was performed on the sample to ensure maintaining the total areal density in the film as it enters the data analysis and simulations of these experiments (more details in 2.3).

Experimental setup and approaches

The ToF-LEIS setup at Uppsala University (ACOLISSA [13]) can provide primary ion beams within the energy range of 0.5 – 10 keV out of gaseous sources like H, D, He and Ne, as well as molecular beams such as H_2^+ and D_3^+. The backscattered ions are detected by a set of two microchannel plates in a chevron stack configuration at a fixed central angle of 129° covering a solid angle of 2×10^{-4} sr. All the experiments in this work were performed under normal incidence to minimize the potential effects of surface roughness as well as to exploit the 2π symmetry for polycrystalline samples in the evaluations. The recorded charge-integrated spectra are subsequently converted to the energy domain. The system provides a high depth resolution in the monolayer regime [16] and has been earlier employed for obtaining electronic stopping powers from the energy width of spectra in backscattering geometry [17] as well as the intensity of charge normalized backscattering spectra [18].

Relative measurements have been shown to provide access to the electronic stopping power also for slow ions by measuring the intensity of spectra recorded in backscattering geometry from bulk samples [19] relative to a standard material with well-known specific electronic energy loss. In this approach, there is a reduced need for accurate knowledge of a number of relevant experimental parameters such as sample thickness. The feasibility of this approach for the specific material system of W is due to the fact that Au can be used as a reference system, as it features a well-known electronic stopping cross section ε [17,20], which is required in the evaluation routine (more details in 2.3). Au, due to its proximity in atomic mass to that of W, features similar scattering kinetics, multiple scattering and possible correction factors for the scattering potential, thus reducing probable systematic uncertainties in the analysis. In this approach, to meet the requirement of the same irradiation fluence on each sample for reliable analysis, the ToF-LEIS spectra were acquired in 10 alternate cycles of identical exposure time on W and Au. A sum of all the 10 spectra recorded for W and for Au, separately, was used in the evaluation routine for each energy-ion case. The number of total counts for each spectrum was compared, and the averaged statistical scatter of the mean values for all integrated spectra was evaluated to be in the range of 1 to 5%. This contribution was included in the final uncertainty considering statistical and systematic uncertainties. The primary energies employed for H_2^+ were within 1.5 – 10 keV, and for He^+ ions were in the range of 0.6 – 10 keV.

For the absolute measurements, mainly the thin films deposited on carbon substrate were employed due to the better mass separation in the resulting ToF-LEIS spectra. One set of measurements was done on thin films on a silicon substrate showing no notable change in the quality of acquired ToF-LEIS spectra and obtained electronic stopping cross sections. The employed primary energies in the presented experiments were 0.3 – 10 keV for protons, 0.33 – 10 keV for deuterons, and 0.7 – 10 keV for He^+ ions.

Evaluation routines

In the case of relative measurements, the relevant parameter is the charge normalized intensity of the energy-converted spectrum as it contains information on ε of the target material for incoming ions along their trajectories in the target (see Fig. 1). A quantitative evaluation of ε for each pair of W and Au spectra is facilitated by comparing the experimental height ratios to the ratios obtained from corresponding Monte Carlo simulations using the TRim for BackScattering ions (TRBS) code [21] where the only free variable was ε_W. In the simulations, which are performed to account for contributions from plural and multiple scattering, the screened Universal potential (ZBL) with the Universal screening length model was used. The energy interval to compare the heights of W and Au spectra was selected close to the signal originating from the surface so that the effects of multiple scattering are alleviated

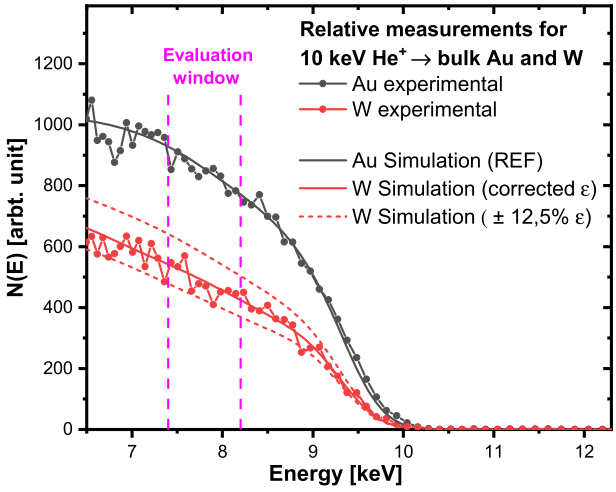

Fig. 1. Experimental spectra of 10 keV primary He^+ ions scattered from bulk Au and W samples, as well as their corresponding TRBS simulations using recently experimentally deduced ε_{Au} [17,24] and the optimum corrected ε_W, for Au in black and W in red, respectively. The evaluation window is indicated by pink dashed lines. The red dash lines demonstrate the sensitivity of the spectrum height to changes in SCS.

[22] and narrow enough in energy to make sure the specific energy loss has sufficient linearity to energy. Linearity is important when calculating the average energy and the respective average deduced ε_W to report, in other words, $\bar{E} = (E^i + E^f)/2$ and $\bar{\varepsilon_W} = (\varepsilon_W^i + \varepsilon_W^f)/2$ where i and f denote the initial and final energies of the investigated energy interval, respectively. A more detailed description of this evaluation method can be found in [23]. Fig. 1 presents an example of the relative approach regarding 10 keV He^+ on bulk Au (in black line + symbol) and W (in red line + symbol). The black and red solid lines are the TRBS simulations using the recent experimentally deduced ε_{Au} [17,24] and the optimum corrected ε_W, for Au and W respectively. The energy interval chosen for the evaluation routine, according to the criteria explained earlier in 2.3, is shown with pink dashed lines. The red dashed lines show TRBS simulations using ± 12.5% ε_W to demonstrate the sensitivity of the height of the spectra to the SCS.

In the absolute measurements, ε_W is extracted from the width of the energy-converted spectrum (see Fig. 2). In this approach, we rely on an accurate areal density of the film, measured by RBS and evaluated using SIMNRA [25], as an input for the TRBS simulations and a good fit of the simulations to the experiment on the high-energy and low-energy edges of the plateau in the energy-converted spectrum. The high-energy edge represents mainly single scattered projectiles from the surface of the film [21]. Thomas-Fermi-Molière potential with the Firsov screening length model was used to account for multiple scattering, and the only free parameter in simulations was ε_W. It is worth noting that the specific choice of potential has no significant effect on the simulations for both cases. This will generally apply to the relative approach as the ratio of the spectra heights is employed, consequently effectively cancelling out the effect of the potential on the height of spectra for target elements close in atomic number. For all calculated spectra, 10 million primary ions with an incident angle of 0°, equal to the angle used in the experiments were simulated. The typical final set energy in the simulations was 10% of the initial energy using a cut-off angle of 2°, meaning only scattering events with an angle above 2° are explicitly calculated with the events below 2° being considered via an analytic correction [21]. One example of an absolute measurement is illustrated in Fig. 2. The gray line + symbol shows the experimental spectrum for 1.2 keV H_2^+ on a 3.52 nm W film on a carbon substrate. The blue solid line represents the best fit using an optimum corrected ε_W in the respective TRBS simulation. The sensitivity of the spectrum width to the SCS is demonstrated by two blue dashed lines representing TRBS simulations using ± 10% ε_W. The black dashed line labeled as KE_0 marks the energy of a proton with the initial energy of 600 eV inelastically scattered on a W atom at a scattering angle of 129°. Here, K stands for the kinematic factor and E_0 denotes the initial energy. The evaluation routines mentioned in 2.3 were performed on all the measured data points using protons, deuterons and helium ions for both approaches, presented in the following section.

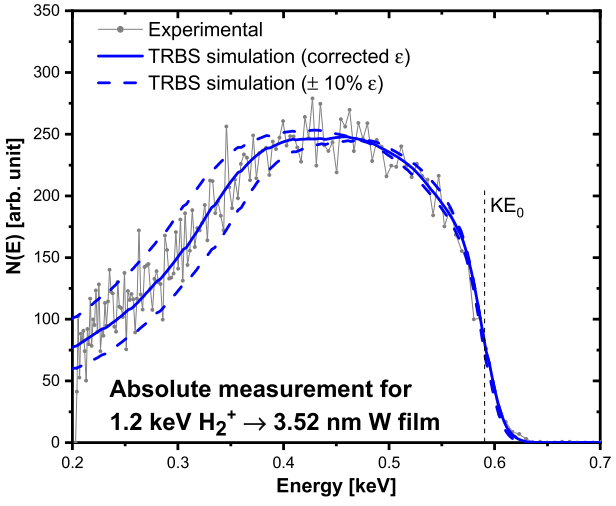

Fig. 2. The experimental spectrum for 1.2 keV H_2^+ on a 3.6 nm W film. The blue solid line represents the best fit using an optimum corrected ε_W in the respective TRBS simulation. The two blue dashed lines represent TRBS simulations using ± 10% ε_W exhibiting the sensitivity of the spectrum width to the SCS. The black dashed line labeled as KE_0 marks the expected energy of a proton with the initial energy of 600 eV elastically scattered from a W atom in a scattering angle of 129°. Here, K stands for the kinematic factor and E_0 denotes the initial energy.

Results and discussion

The compiled deduced SCS of W from both relative and absolute approaches are plotted as a function of their corresponding ion velocity in Fig. 3 for protons and deuterons and in Fig. 4 for helium ions. In both Fig. 3 and Fig. 4, two data points from Moro et al. [26] are included which is the dataset featuring the lowest available energies on the IAEA database.

In Fig. 3, the ε_W for protons and deuterons from absolute measurements are indicated by open squares and circles, respectively, with 3 – 5% uncertainty, due to fitting accuracy and potential inaccuracies in film thickness. The open triangles represent the ε_W for protons from relative measurements with 5% uncertainties, mainly due to fitting accuracy and fluctuations in the beam current affecting the assumed identical charge × solid angle product. Open asterisks are the data points for protons taken from [26] including approx. 3% uncertainty which show good agreement with the presented data in this work. Additionally, SRIM 2013 [6] semiempirical model in green solid line, Montanari 2009 [27] ab initio theoretical calculations in violet dashed line, ESPNN [28] neural-network predictions based on the available experimental data on the IAEA database in blue solid line, and CasP [29] fast numerical calculations using the unitary convolution approximation (UCA) and screening function for the mean charge state in pink solid line are provided in Fig. 3 to compare the experimental data to the existing models.

In Fig. 4, the ε_W for helium ions from absolute and relative measurements are illustrated by open squares (± 3 – 6%) and triangles (± 8%), respectively. The open asterisks are the data points for He^+ ions taken from [26] agreeing with the results of this work. The predictions by theoretical models such as DPASS 2.0 [30] in magenta dash-dot-dot

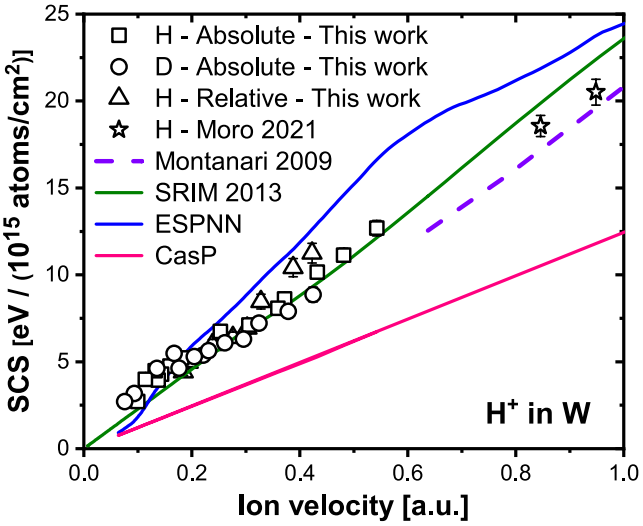

Fig. 3. The compiled deduced SCS of W for protons and deuterons from both relative and absolute approaches as a function of equivalent proton velocity compared to data points from [26]. Existing models such as SRIM 2013, Montanari 2009, ESPNN and CasP are included for comparison.

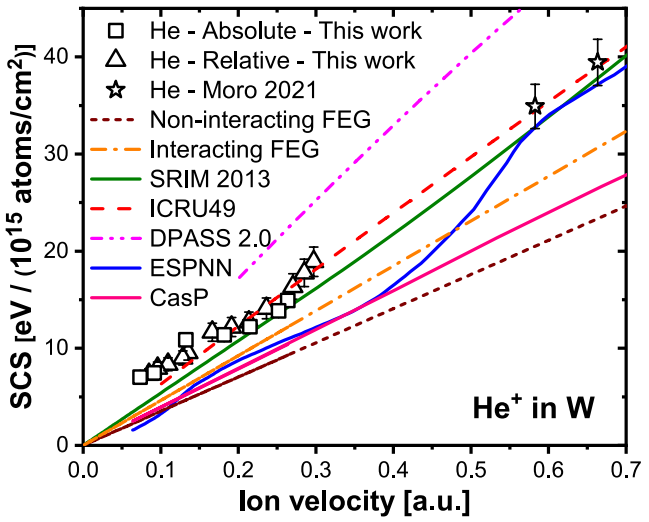

Fig. 4. The compiled deduced SCS of W for He^+ ions from both relative and absolute approaches as a function of helium velocity compared to data points from [26]. Existing models such as SRIM 2013, ICRU49, DPASS 2.0, ESPNN, CasP, as well as DFT predictions for a free electron gas, are included for comparison. See the text for more details.

line, as well as SRIM 2013 [6] in green solid line, ESPNN [28] neural-network predictions in blue solid line, ICRU 49 [31] semiempirical model in red dashed line, and CasP [29] in pink solid line are included for comparison. The dark red short-dashed line and orange dash-dot line represent the calculations based on non-interacting and interacting electron gas models, respectively. The models were taken from Fig. 2 in [32].

In Figs. 3 and 4, slight differences between the deduced data and predictions by SRIM are observed for the highest investigated energies, while for the lowest investigated energies the difference to SRIM is more notable, going up to 60%. The same observation is true for the ICRU 49 model predictions for He^+ with less differences in total (Fig. 4). The neural-network extrapolations feature large fluctuations due to a lack of experimental data in the low-energy regime on the IAEA database for both protons and helium ions (Figs. 3, 4). Montanari 2009 ab initio calculations cover the energies down to 10 keV for protons only (Fig. 3). DPASS 2.0, binary theory of electronic stopping, covers the upper half of the investigated energies for helium in this work where it significantly overestimates the SCS in comparison to the experiment (Fig. 4). CasP 6.0, fast numerical calculations of the mean electronic energy transfer for each individual impact parameter in a collision, underestimates the SCS for both protons and He ions compared to the present experimental data, given the aforementioned employed conditions (Figs. 3, 4).

For low-energy ions, i.e. ion velocities comparable to or less than the Bohr velocity ($v < v_0$), the electronic SCS is expected to be dominated by the excitation of valence electrons. The free electron gas model (FEG) predicts that at low energies, the electronic SCS is proportional to ion velocity, $\varepsilon = Q(Z_1, r_s)v$, where Q is the friction coefficient that depends on the projectile atomic number (Z_1) and the Wigner-Seitz radius of the target atom $r_s = (3/4\pi n_e)^{1/3}$ with n_e the FEG effective density of target electrons [33]. According to this theory, from a linear fit to our data, $Q = 24.2\ 10^{-15}$eV.cm^2 is obtained resulting in $r_s^{non-int} = 0.94$ Å and $r_s^{int} = 1.13$ Å based on the non-interacting and interacting free electron gas models [32] respectively. Thus, the non-interacting model suggests 4.68 e^-/W-atom and the interacting model gives 2.74 e^-/W-atom. As the target is the same for both protons and He^+ ions, one can utilize the extracted $r_s^{non-int}$ and r_s^{int} from protons and calculate their corresponding friction coefficients for He^+ ions. Hence, $Q^{non-int} = 35.2\,10^{-15}$eV.cm^2 (the dark red short-dashed line in Fig. 4) and $Q^{int} = 46.2\,10^{-15}$eV.cm^2 (the orange dash-dot line in Fig. 4) are obtained according to the non-interacting and interacting free electron gas models [32] respectively. However, both these predictions underestimate the friction coefficient for He^+ ions compared to the experimental data presented in Fig. 4. This discrepancy can be related to the fact that the proton represents a point charge, therefore, no projectile excitation occurs in its interactions. However, helium has a more complex electronic system which offers probabilities for trajectory-dependent electronic excitations during interactions such as charge exchange processes [34,35], resulting in trajectory-dependent energy loss even at low ion energies [36].

The data obtained in this work exhibit deviation from velocity proportionality towards the lowest energies for both protons and helium ions. There are a number of potential systematic uncertainties in the experiments which can contribute to explaining this observation. One option is contaminants incorporated into the near-surface and film-substrate interface region of the film. For thinner films, such effects would become more important and could thus explain the observed deviations. For the near-surface region, however, AES spectra suggest only very minor contributions from foreign atoms. Also, a potential surface roughness, thickness inhomogeneity of the deposited films and/or interface roughness between the substrate and the film could lead to a perceived increase in the energy loss for the lowest physical film thicknesses, as the limited system resolution in the present experiments might make it challenging to distinguish spectral broadening due to film thickness inhomogeneity from effects from plural scattering. For Helium ions, deviations from velocity proportionality observed in the relative approach can also be partially attributed to a potential offset due to the employed ε_{Au} which has been measured using a different approach, i.e. absolute measurements, that due to the demonstrated trajectory dependence of the electronic energy loss could be slightly off for the present approach.

Summary

Time-of-flight low-energy ion scattering (ToF-LEIS) was used to experimentally deduce the electronic stopping cross-section (SCS) of tungsten for low-energy protons, deuterons and helium ions by comparison to Monte Carlo simulations using the TRBS code. Two complementary relative and absolute measurements on bulk and sputter-deposited thin films, respectively, were performed. The compiled results show slight differences from SRIM predictions for the highest investigated energies, whereas the lowest investigated energies exhibit more notable differences. Additionally, the results agree with the free electron gas model predictions regarding the proportionality of the SCS to the ion velocity in the measured energy range.

CRediT authorship contribution statement

Jila Shams-Latifi: Investigation, Methodology, Formal analysis, Validation, Software, Data curation, Writing – original draft, Writing – review & editing, Visualization. **Eduardo Pitthan:** Conceptualization, Methodology, Investigation, Formal analysis, Validation, Software, Data curation, Writing – review & editing, Supervision, Project administration. **Philipp Mika Wolf:** Investigation, Writing – review & editing. **Daniel Primetzhofer:** Conceptualization, Methodology, Resources, Writing – review & editing, Supervision, Project administration, Funding acquisition.

Declaration of Competing Interest

The authors declare that they have no known competing financial interests or personal relationships that could have appeared to influence the work reported in this paper.

Data availability

Data will be made available on request.

Acknowledgement

The authors acknowledge financial support from the Swedish research council, VR-RFI (contract #2017-00646_9 and #2019_00191), and the Swedish Foundation for Strategic Research (SSF, contract RIF14-0053) are acknowledged. This work has been carried out within the framework of the EUROfusion Consortium, funded by the European Union via the Euratom Research and Training Programme (Grant Agreement No 101052200 — EUROfusion). Views and opinions expressed are however those of the author(s) only and do not necessarily reflect those of the European Union or the European Commission. Neither the European Union nor the European Commission can be held responsible for them. Jila Shamslatifi would like to express her gratitude to Dr. Mauricio Sortica and Dr. Robert Frost for their valuable support for the RBS and ERDA experiments.

References

[1] G. Pintsuk, et al., Materials for in-vessel components, Fusion Eng. Des. 174 (2022), 112994, https://doi.org/10.1016/j.fusengdes.2021.112994.
[2] J.H. You, H. Greuner, B. Böswirth, K. Hunger, S. Roccella, H. Roche, High-heat-flux performance limit of tungsten monoblock targets: Impact on the armor materials and implications for power exhaust capacity, Nuclear Materials and Energy 33 (2022), 101307, https://doi.org/10.1016/j.nme.2022.101307.
[3] K. Nordlund, et al., Primary radiation damage: A review of current understanding and models, J. Nucl. Mater. 512 (2018) 450–479, https://doi.org/10.1016/j.jnucmat.2018.10.027.
[4] A.E. Sand, "Incorporating Electronic Effects in Molecular Dynamics Simulations of Neutron and Ion-Induced Collision Cascades", in Handbook of Materials Modeling, Springer International Publishing (2018) 1–25, https://doi.org/10.1007/978-3-319-50257-1_135-1.
[5] IAEA Nuclear Data Section, "Electronic Stopping Power of Matter for Ions", Accessed: Mar. 10, 2023. [Online]. Available: https://www-nds.iaea.org/stopping/index.html.
[6] J.F. Ziegler, M.D. Ziegler, J.P. Biersack, SRIM - The stopping and range of ions in matter (2010), Nucl Instrum Methods Phys Res B 268 (2010) 1818–1823, https://doi.org/10.1016/j.nimb.2010.02.091.
[7] M.V. Moro, P. Bauer, D. Primetzhofer, Experimental electronic stopping cross section of transition metals for light ions: Systematics around the stopping maximum, Phys. Rev. A 102 (2020), 022808, https://doi.org/10.1103/PhysRevA.102.022808.
[8] D. Roth, et al., Electronic Stopping of Slow Protons in Transition and Rare Earth Metals: Breakdown of the Free Electron Gas Concept, Phys. Rev. Lett. 118 (2017), 103401, https://doi.org/10.1103/PhysRevLett.118.103401.
[9] F. Matias, P.L. Grande, M. Vos, P. Koval, N.E. Koval, N.R. Arista, Nonlinear stopping effects of slow ions in a no-free-electron system: Titanium nitride, Phys. Rev. A 100 (2019), 030701, https://doi.org/10.1103/PhysRevA.100.030701.
[10] R. Ullah, E. Artacho, A.A. Correa, Core Electrons in the Electronic Stopping of Heavy Ions, Phys. Rev. Lett. 121 (2018), 116401, https://doi.org/10.1103/PhysRevLett.121.116401.
[11] S.M. Li, et al., First-principles study of the electronic stopping power of indium for protons and He ions, Phys. Rev. B 104 (2021), 214104, https://doi.org/10.1103/PhysRevB.104.214104.
[12] E.E. Quashie, R. Ullah, X. Andrade, A.A. Correa, Effect of chemical disorder on the electronic stopping of solid solution alloys, Acta Mater. 196 (2020) 576–583, https://doi.org/10.1016/j.actamat.2020.06.061.
[13] M. Draxler, et al., ACOLISSA: A powerful set-up for ion beam analysis of surfaces and multilayer structures, Vacuum 73 (2004) 39–45, https://doi.org/10.1016/j.vacuum.2003.12.041.
[14] P. Ström, D. Primetzhofer, Ion beam tools for nondestructive in-situ and in-operando composition analysis and modification of materials at the Tandem Laboratory in Uppsala, J. Instrum. 17 (2022) P04011, https://doi.org/10.1088/1748-0221/17/04/P04011.
[15] E. Pitthan, et al., Thin films sputter-deposited from EUROFER97 in argon and deuterium atmosphere: Material properties and deuterium retention, Nuclear Materials and Energy 34 (2023), 101375, https://doi.org/10.1016/j.nme.2023.101375.
[16] D. Primetzhofer, et al., Quantitative analysis of ultra thin layer growth by time-of-flight low energy ion scattering, Appl. Phys. Lett. 92 (2008), 011929, https://doi.org/10.1063/1.2822816.
[17] S.N. Markin, D. Primetzhofer, M. Spitz, P. Bauer, Electronic stopping of low-energy H and He in Cu and Au investigated by time-of-flight low-energy ion scattering, Phys. Rev. B: Condens. Matter Mater. Phys. 80 (2009), 205105, https://doi.org/10.1103/PhysRevB.80.205105.
[18] D. Goebl, D. Roth, P. Bauer, Role of d electrons in electronic stopping of slow light ions, Phys. Rev. A 87 (2013), 062903, https://doi.org/10.1103/PhysRevA.87.062903.
[19] D. Roth, D. Goebl, D. Primetzhofer, P. Bauer, A procedure to determine electronic energy loss from relative measurements with TOF-LEIS, *Nucl. Instrum. Methods Phys Res B*, 317 Part A (2013) 61–65, https://doi.org/10.1016/j.nimb.2012.12.094.
[20] J.E. Valdes, J.C. Eckardt, G.H. Lantschner, N.R. Arista, G. Martinez-Tamayo, Energy loss of slow protons in solids: Deviation from the proportionality with projectile velocity, Phys. Rev. A 49 (1994) 1083, https://doi.org/10.1103/PhysRevA.49.1083.
[21] J.P. Biersack, E. Steinbauer, P. Bauer, A particularly fast TRIM version for ion backscattering and high energy ion implantation, Nucl Instrum Methods Phys Res B 861 (1991) 77–82, https://doi.org/10.1016/0168-583X(91)95564-T.
[22] B. Bruckner, T. Strapko, M.A. Sortica, P. Bauer, D. Primetzhofer, On the influence of uncertainties in scattering potentials on quantitative analysis using keV ions, Nucl Instrum Methods Phys Res B 470 (2020) 21–27, https://doi.org/10.1016/j.nimb.2020.02.018.
[23] M.V. Moro, B. Bruckner, P.L. Grande, M.H. Tabacniks, P. Bauer, D. Primetzhofer, Stopping cross section of vanadium for H+ and He+ ions in a large energy interval deduced from backscattering spectra, Nucl Instrum Methods Phys Res B 424 (2018) 43–51, https://doi.org/10.1016/j.nimb.2018.03.032.
[24] D. Primetzhofer, Inelastic energy loss of medium energy H and He ions in Au and Pt: Deviations from velocity proportionality, Phys. Rev. B: Condens. Matter Mater. Phys. 86 (2012), 094102, https://doi.org/10.1103/PhysRevB.86.094102.
[25] M. Mayer, SIMNRA, a simulation program for the analysis of NRA, RBS and ERDA, AIP Conference Proceedings 475 (1999) 541–544, https://doi.org/10.1063/1.59188.
[26] M.V. Moro, et al., Experimental electronic stopping cross section of tungsten for light ions in a large energy interval, Nucl Instrum Methods Phys Res B 498 (2021) 1–8, https://doi.org/10.1016/j.nimb.2021.04.010.
[27] C.C. Montanari, D.M. Mitnik, C.D. Archubi, J.E. Miraglia, Energy loss of protons in W using fully relativistic calculations and mean excitation energies of W, Au, Pb, and Bi, Phys. Rev. A 80 (2009), 012901, https://doi.org/10.1103/PhysRevA.80.012901.
[28] F. Bivort Haiek, A.M.P. Mendez, C.C. Montanari, D.M. Mitnik, ESPNN: A novel electronic stopping power neural-network code built on the IAEA stopping power database. I. Atomic targets, J Appl Phys 132 (2022), 245103, https://doi.org/10.1063/5.0130875.
[29] F. Matias, R.C. Fadanelli, P.L. Grande, N.R. Arista, N.E. Koval, G. Schiwietz, Stopping power of cluster ions in a free-electron gas from partial-wave analysis, Phys. Rev. A 98 (2018), 062716, https://doi.org/10.1103/PhysRevA.98.062716.
[30] A. Schinner, P. Sigmund, Expanded PASS stopping code, Nucl Instrum Methods Phys Res B 460 (2019) 19–26, https://doi.org/10.1016/j.nimb.2018.10.047.
[31] M.J. Berger, et al., Report 49, stopping powers and ranges for protons and alpha particles, Oxford Academic (1993), https://doi.org/10.1093/JICRU/OS25.2.REPORT49.
[32] I. Nagy, A. Arnau, P.M. Echenique, Nonlinear stopping power and energy-loss straggling of an interacting electron gas for slow ions, Phys. Rev. A 40 (1989) 987, https://doi.org/10.1103/PhysRevA.40.987.
[33] D. Roth, et al., Electronic Stopping of Slow Protons in Oxides: Scaling Properties, Phys. Rev. Lett. 119 (2017), 163401, https://doi.org/10.1103/PhysRevLett.119.163401.
[34] S. Rund, D. Primetzhofer, S.N. Markin, D. Goebl, P. Bauer, Charge exchange of He +-ions with aluminium surfaces, Nucl Instrum Methods Phys Res B 269 (2011) 1171–1174, https://doi.org/10.1016/j.nimb.2010.11.049.
[35] D. Primetzhofer, D. Goebl, P. Bauer, Local vs. non-local energy loss of low energy ions: Influence of charge exchange processes in close collisions, *Nucl. Instrum. Methods Phys Res B*, 317 PartA (2013) 8–12, https://doi.org/10.1016/j.nimb.2012.12.091.
[36] S. Lohmann, D. Primetzhofer, Disparate energy scaling of trajectory-dependent electronic excitations for slow protons and He Ions, Phys. Rev. Lett. 124 (2020), 096601, https://doi.org/10.1103/PhysRevLett.124.096601.